Volume 47
Number 7
21 February 2023
Pages 3187–3636

NJC

New Journal of Chemistry

A journal for new directions in chemistry

rsc.li/njc

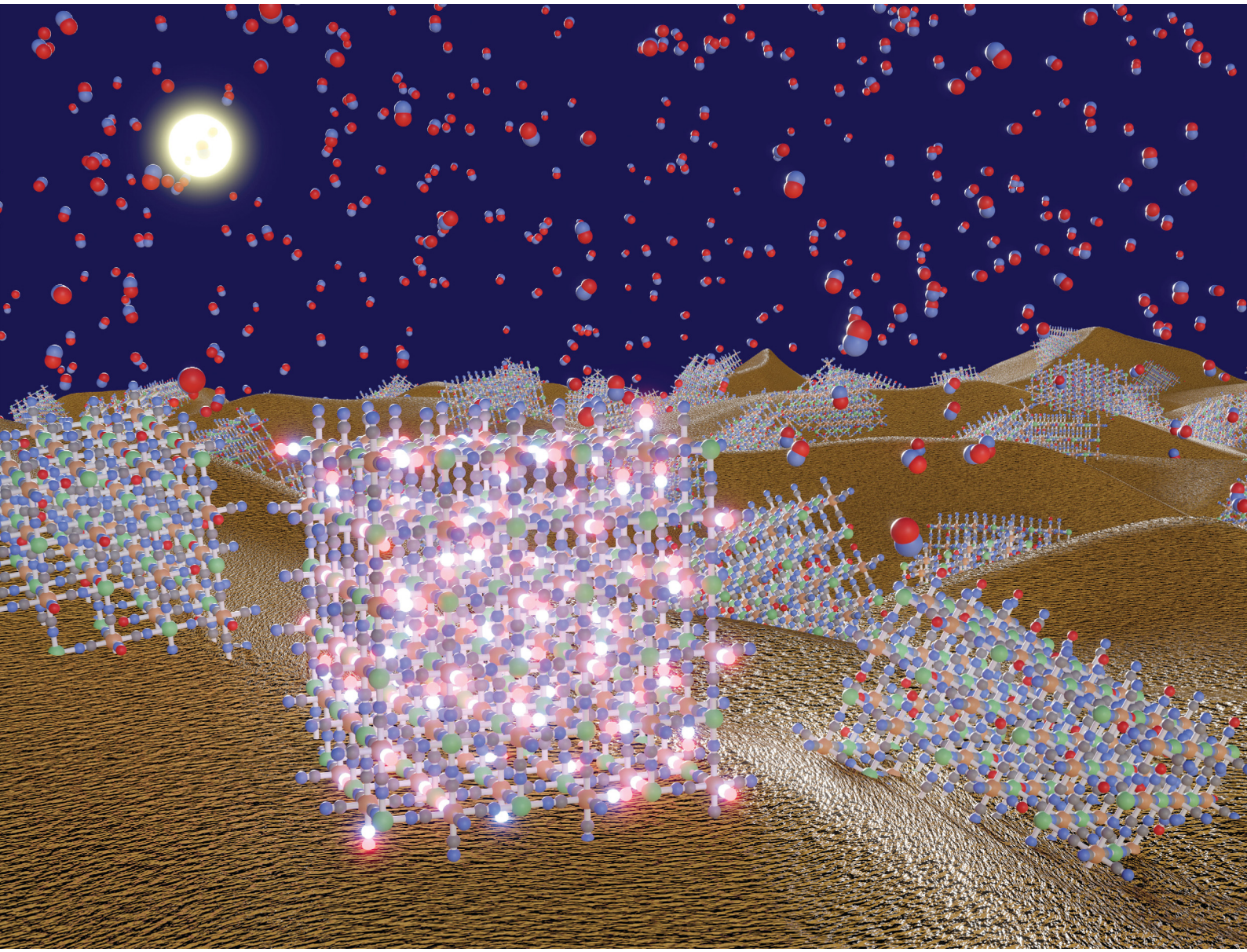

ISSN 1144-0546

ROYAL SOCIETY OF CHEMISTRY

PAPER

Joulia Larionova, Yannick Guari *et al.*
Composites based on nitroprusside cyano-bridged coordination polymer particles and chitosan for NO delivery

cnrs

NJC

ROYAL SOCIETY OF CHEMISTRY

PAPER

View Article Online
View Journal | View Issue

Cite this: *New J. Chem.*, 2023, **47**, 3207

Composites based on nitroprusside cyano-bridged coordination polymer particles and chitosan for NO delivery†

Melvyn Gorra, Frantz Ndebulia Watchou, Maria A. Palacios, ‡ Jérôme Long, Saad Sene, Gautier Félix, Nathalie Tanchoux, Françoise Quignard, Joulia Larionova * and Yannick Guari *

Received 23rd September 2022,
Accepted 28th November 2022

DOI: 10.1039/d2nj04711j

rsc.li/njc

We report the design of new composite films $\{Fe[Fe(CN)_5(NO)]\}_{0.55}@C_6H_{11}NO_4$ and $\{Ag_2[Fe(CN)_5(NO)]\}_{0.28}@C_6H_{11}NO_4$ based on cyano-bridged coordination polymers $Fe^{II}[Fe^{II}(CN)_5(NO)]$ or $Ag_2^{I}[Fe^{II}(CN)_5(NO)]$ grown into a chitosan matrix that are able to provide a slow NO radical release under white light irradiation. The characterisation methods such as X-ray diffraction, TGA, SEM-EDX, IR and UV-vis spectroscopies show that these composites are made of *ca.* 50 wt% of the cyano-bridged coordination polymer as microcrystalline particles embedded into chitosan films. Irradiation for 7 days by using white light results in initiating a 6.5 and 10.6% NO radical delivery for $\{Fe[Fe(CN)_5(NO)]\}_{0.55}@C_6H_{11}NO_4$ and $\{Ag_2[Fe(CN)_5(NO)]\}_{0.28}@C_6H_{11}NO_4$, respectively. The rearrangement of the cyano-bridged coordination compounds after the NO departure leads to the formation of Prussian blue or silver Prussian blue analogues, which limits the unwanted release of cyanide as a side effect.

Introduction

Nitric oxide (NO) is a gaseous radical molecule possessing numerous biological functions including gene regulation, vasorelaxation, vascular permeability, bronchodilatation, platelet aggregation, angiogenesis, neuronal communication, hormone secretion, immune system regulation, inflammation and wound healing. Therefore, delivery of a controlled, quantifiable and biologically significant amount of NO is attractive for many *in vitro* and *in vivo* applications, such as curative,[1–4] antithrombotic,[5] anti-inflammatory, and antibiotic-based therapies.[6–9] However, its short half-life (between 0.1 and 5 s in aqueous solutions), high chemical reactivity, rapid systemic clearance, instability under physiological conditions, lipophilicity and cytotoxicity make the direct delivery of nitric oxide using classical methods very difficult.[10] Furthermore, for certain applications, the kinetics of NO delivery must be slow. This is particularly the case for the treatment of chronic wounds for which the inflammatory phase lasts too long to allow proper healing.[11]

The employment of composite materials allowing the generation of NO *in situ* and therefore providing its controlled and local release (not systemic) has emerged as a unique strategy for the safe nitric oxide delivery reducing indeed unwanted side effects.[10] These materials usually encapsulate organic NO-donor molecules, such as *S*-nitrosothiols[12] and *N*-diazeniumdiolates, or nitrosylmetal complexes[13] into the host matrixes.[14] We can cite micro- and nano-scale materials, including functionalized polymers or dendrimers,[15–17] silica nanoparticles,[18,19] zeolites,[20] gold clusters,[21] or metal–organic frameworks,[22,23] developed in the recent years, capable of producing and releasing NO at different rates and in different amounts. However, many of these employed organic NO donors suffer from carcinogenic or pro-inflammatory side products, which may limit their applicability.

An alternative nitric oxide source is well-known under the name of sodium nitroprusside with the chemical formula $Na_2[Fe(CN)_5NO]\cdot 2H_2O$, for which the hypotensive action linked with the NO release has been demonstrated first in 1929. Indeed, the aqueous solution of this compound is widely used in the clinical practice to induce hypotension during surgery through a fine control of its infusion rate, which allows adjustment of the blood pressure in a very effective and fast response without overshoot.[24] Similarly, nitroprusside is used in the treatment of chronic hypertension, in the management of myocardial infarction and other cardiac failures. It is capable of releasing NO enzymatically and non-enzymatically when in

ICGM, University Montpellier, CNRS, ENSCM, Montpellier, 34000, France. E-mail: joulia.larionova@umontpellier.fr, yannick.guari@umontpellier.fr

† Electronic supplementary information (ESI) available. See DOI: https://doi.org/10.1039/d2nj04711j

‡ Current address: Departamento de Química Inorgánica, Facultad de Ciencias, Universidad de Granada, 18071 Granada, Spain.

the presence of vascular tissue and reducing agents or activated by light irradiation with the quantity of 1 mole of NO per mole of nitroprusside.[25] However, the employment of nitroprusside is restricted because the NO delivery is accompanied by compound decomposition inducing the liberation of free cyanides. Moreover, another important disadvantage of employing nitroprusside is its instability in aqueous solutions when exposed to light and therefore the impossibility of the slow and controlled NO delivery. In order to overcome this problem, several works have reported the encapsulation of nitroprusside into silica nanoparticles in order to protect this fragile compound and provide the *in situ* NO delivery in aqueous solutions.[18,19]

Another option to render nitroprusside more stable is *via* its integration as a building block in cyano-bridged coordination polymers of general formula $M_x[Fe^{II}(CN)_5(NO)]$ (where M = mono- (x = 2) or bivalent (x = 1) metal ions). These bulk compounds present a cubic structure (*Fm3m* space group) for M = bivalent transition metal ions[26] and a monoclinic one (*Pc* space group) for M = monovalent ions.[27] Recently, the photodegradation of these compounds in water under irradiation by white light has been investigated and a structural re-organisation to Prussian blue or its analogues occurred after irradiation and the NO departure has been demonstrated by means of infrared and Mössbauer spectroscopy.[28] However, to the best of our knowledge, these coordination polymers have never been proposed as a source of NO and the kinetic monitoring of the NO release has never been investigated. Also note that the design of composite materials involving $M_x[Fe^{II}(CN)_5(NO)]$ coordination polymers has never been reported till date.

In this article, we describe the synthesis and characterisation of new composite materials based on coordination polymer particles, $M_x[Fe^{II}(CN)_5(NO)]$ (where M = Fe^{2+} or Ag^+), embedded into chitosan polysaccharide films and their ability to slowly deliver NO under white light irradiation. Chitosan was chosen here as a matrix because it is a non-toxic, biocompatible, biodegradable and a bioactive polymer derived from the partial deacetylation of chitin, which is approved for use on human beings.[29,30] Furthermore, it can be shaped in the form of beads or films, still exhibiting a porous structure when dried under supercritical CO_2 conditions[31] or as an alcogel.[32] Thanks to the accessible free amino groups that are able to coordinate with metal ions, it was successfully used in the covalent anchoring of cyano-bridged coordination networks.[33–38] We focus here on the growth of $Fe^{II}[Fe^{II}(CN)_5(NO)]$ and $Ag_2^I[Fe^{II}(CN)_5(NO)]$ particles into chitosan films because: (i) we expect that these particles will *in situ* produce the NO radicals under appropriate irradiation and (ii) we expect that NO departure will induce structural reorganisation and formation of biocompatible Prussian blue or Ag^+-based Prussian blue analogue particles avoiding a huge CN^- release unsuitable for biomedical applications. Indeed, in comparison with $M[Fe^{II}(CN)_5(NO)]$ analogous with M = Mn^{2+}, Zn^{2+}, Cd^{2+} and alkali metal ions, the cyano-bridged networks of M = Fe^{2+} and Ag^+ are robust, insoluble in water and thus more resistant to degradation.[28] Particular attention is paid to the kinetics of NO delivery during the light exposure in the solid state and in solution, as well as to the resulting rearrangement of the cyano-bridged coordination networks affording the formation of the corresponding Prussian blue or Ag^+ Prussian blue analogues without significant leaching of cyanide.

Experimental

Synthetic procedures

Synthesis of $Na_{0.04}Fe[Fe(CN)_5NO]$ 1. The synthesis of cyano-bridged network material **1** was performed by adding dropwise 100 mL of an aqueous solution of $Na_2[Fe(CN)_5NO]\cdot 2H_2O$ (5×10^{-2} M) into 100 mL of an aqueous solution of $FeCl_2\cdot 4H_2O$/ascorbic acid (5×10^{-2} M each) leading to the formation of a brown precipitate. The mixture was stirred for one hour before being centrifuged at 35 700 × g (20 000 rpm) for 10 min. The supernatant was removed and the brown solid was washed twice with water and dried under vacuum.

IR (cm^{-1}): 3844 overtone ν(NO), ν(OH): 3659 and 3387, ν(CN):2182 and 2147, ν(NO): 1941, δ(OH): 1616, δ(Fe–NO): 666, ν(Fe–CN): 520, δ(Fe–CN): 443. TGA analysis: 30–150 °C (23.4 wt%), 240 °C (11.3 wt%), 301 °C (11.9 wt%), 343 °C (6.1 wt%), 520 °C (3 wt%); residual mass 55 wt%. SEM-EDS (at%): Na/Fe = 2/98, estimated formula $Na_{0.04}Fe[Fe(CN)_5(NO)]$. UV-Vis spectroscopy: wide absorption 230–700 nm, maximums at 260, 338, 465 nm. XRD (2θ, *hkl*): 17.25° (002), 24.40° (022), 30.01° (222), 34.78° (004), 39.01° (024), 42.89° (224), 49.92° (044), 53.20° (006) 56.36° (026); cubic structure, estimated cell parameter a = 10.35 Å.

Synthesis of $Ag_2[Fe(CN)_5NO]$ 2. The synthesis of cyano-bridged network material **2** obtained as a light pink powder was performed using the same method as described above for $Na_{0.04}Fe[Fe(CN)_5NO]$ by replacing $FeCl_2\cdot 4H_2O$/ascorbic acid by 2 equivalents of $AgNO_3$.

IR (cm^{-1}): 3854 overtone ν(NO),[39] ν(OH): 3443, ν(CN):2177 and 2163, ν(NO): 1937, δ(OH): 1625, δ(Fe–NO): 662, ν(Fe–CN): 516, δ(Fe–CN): 418. TGA (weight loss): 30–238 °C (15.1 wt%), 270 °C (4.5 wt%), 320 °C (8.1 wt%), 450 °C (10.3 wt%); residual mass 62 wt%. SEM-EDS (at%): Na/Ag/Fe = 0/67/33, estimated formula $Ag_2[Fe(CN)_5(NO)]$. UV-Vis spectroscopy: wide absorption 230–650 nm, maximums at 262, 300, 401, 534 nm. XRD (2θ, *hkl*): 13.23° (100), 13.84° (010), 16.18° (011), 18.50° (−1–11), 19.17° (110), 21.35° (−112), 21.61° (012), 24.51° (−202), 25.27° (102), 26.57° (200), 27.84° (020), 28.57° (013), 29.05° (021), 30.01° (−104), 30.95° (120), monoclinic structure, estimated cell parameters a = 7.4412(6) Å, b = 6.4141(1) Å, c = 11.8732(2) Å, β = 115.297(2)°.

Synthesis of a chitosan film. An aqueous solution of chitosan (2.5 wt%) was obtained by dissolving 1 g of chitosan in 40 mL of a solution of acetic acid (1.0 vol%) with magnetic stirring for one night at room temperature. A filter paper (60 mm diameter) was impregnated in NaOH solution (2 M) and put in a Petri dish (60 mm diameter). The chitosan solution (6.5 mL) was then added on the filter paper before being covered by a second filter paper impregnated in NaOH and

3 mL of NaOH solution was added. After 1 hour of gelation, the film was washed in distilled water until pH 6–7 to obtain a hydrogel. The alcogel film was then obtained by the immersion of the hydrogel in a series of successive methanol–water baths of increasing alcohol concentrations (10, 30, 50, 70, 90, and 100 vol%) for 15 min each. The as-obtained chitosan film was then stored in methanol or dried under air for characterization.

Synthesis of $\{Fe[Fe(CN)_5(NO)]\}_{0.55}@C_6H_{11}NO_4$ 1@chit and $\{Ag_2[Fe(CN)_5(NO)]\}_{0.28}@C_6H_{11}NO_4$ 2@chit composites films. The synthesis of composite **1@chit** was performed by growing the cyano-bridged network within the chitosan film as follows: 15 mL of a methanolic solution of $FeCl_2{\cdot}4H_2O$/ascorbic acid (1×10^{-2} M each) was added in a Petri dish containing an alcogel chitosan film and kept under stirring for 48 hours at room temperature. The film was then removed and washed three times with methanol for 15 min before being mixed with 15 mL of a methanolic solution of $Na_2[Fe(CN)_5NO]{\cdot}2H_2O$ (5×10^{-2} M) for 48 hours at room temperature. The consecutive treatment with methanolic solutions of $FeCl_2{\cdot}4H_2O$/ascorbic acid (1×10^{-2} M each) and $Na_2[Fe(CN)_5NO]{\cdot}2H_2O$ was repeated twice (with intermediate washings at each step) to obtain the $\{Fe[Fe(CN)_5(NO)]\}_{0.55}@C_6H_{11}NO_4$ composite as a brown film after air drying.

IR (cm^{-1}): 3838 overtone ν(NO),[39] ν(OH): 3431, ν(CH): 2917, ν(CN): 2182 and 2145, ν(NO): 1941, ν(CO): 1654, δ(NH): 1525, ν(CO): 1080, δ(Fe–NO): 664, ν(Fe–CN): 522, δ(Fe–CN): 431. SEM-EDX (at%): Na/Fe = 0/100. TGA (weight loss): 30–170 °C (9.48 wt%), 283 °C (47.4 wt%), 356 °C (18.1 wt%), 600 °C (3.6 wt%); estimated amount of particles in the composite film is 48 wt%. Estimated formula $\{Fe[Fe(CN)_5(NO)]\}_{0.55}@C_6H_{11}NO_4$. UV-Vis spectroscopy: wide absorption 230–750 nm, maximums at 264, 376, 573 nm. XRD (2θ): 17.13°, 24.28°, 29.88°, 34.65°, 38.95°, 42.89°, 49.92°, 53.14°, 56.18°; cubic structure, estimated cell parameter a = 10.35 Å.

$\{Ag_2[Fe(CN)_5(NO)]\}_{0.28}@C_6H_{11}NO_4$ composite film **2@chit** was obtained as a light pink film following the same method as described above for $\{Fe[Fe(CN)_5(NO)]\}_{0.55}@C_6H_{11}NO_4$ by replacing $FeCl_2{\cdot}4H_2O$/ascorbic acid by $AgNO_3$ (1×10^{-2} M).

IR (cm^{-1}): 3844 overtone ν(NO), ν(OH): 3410, ν(CH): 2920, ν(CN) = 2177 and 2141, ν(NO): 1924, ν(CO): 1644, δ(NH): 1543, ν(CO): 1053, δ(Fe–NO): 659, ν(Fe–CN): 507, δ(Fe–CN): 414. SEM-EDX (at%): Na/Ag/Fe = 0/66/34. TGA (weight loss): 30–228 °C (15.4 wt%), 285 °C (15.2 wt%), 358 °C (10.3 wt%), 412 °C (36.4 wt%); estimated amount of particles in the composite film 41 wt%.

Estimated formula $\{Ag_2[Fe(CN)_5(NO)]\}_{0.28}@C_6H_{11}NO_4$. UV-Vis spectroscopy: wide absorption 230–650 nm, maximums at 260, 379 nm. XRD (2θ): 13.82°, 19.13°, 20.88°, 24.09°, 26.72°, monoclinic structure, estimated cell parameters a = 7.483(6) Å, b = 6.299(2) Å, c = 12.669(6) Å, β = 114.77(3).

Materials and methods

All of the chemical reagents were used as received: chitosan (low molecular weight, deacetylation ≥75%, viscosity: 20–300 cps with 1% in 1% acetic acid, Aldrich), sodium nitroprusside dehydrate, SNP ($Na_2[Fe(CN)_5NO]{\cdot}2H_2O$ 99%, Aldrich), silver nitrate ($AgNO_3$, 99 + %, Alfa Aesar), sodium hydroxide (NaOH 97%, Honeywell), $FeCl_2{\cdot}4H_2O$ (98%, Alfa Aesar), ascorbic acid (99%, Aldrich), acetic acid (Aldrich), methanol (Carlo Erba), *N*-(1-naphthyl)ethylenediamine dehydrochloride (98%, Aldrich), and sulfanilamide (99%, Aldrich).

Physico-chemical characterisation

Infrared spectra were recorded as KBr disks on a PerkinElmer Spectrum two spectrophotometer. UV-Vis spectra were collected on a JASCO V-650 spectrometer. Powder X-ray diffraction (PXRD) patterns were recorded in the 2θ interval 10–60° at room temperature using a PANalytical X'Pert Powder analytical diffractometer mounted in a Debye–Scherrer configuration and equipped with Cu radiation (λ = 1.5418 Å). Thermogravimetric analysis (TGA) was performed with a thermal analyser STA 409 Luxx (Netzsch) in the range of 25–800 °C at a heating speed of 2 °C min^{-1} under air flow (~60 mL min^{-1}). Scanning electronic microscopy coupled with energy dispersive X-ray spectroscopy (SEM-EDX) analyses were performed on a FEI Quanta FEG 200 instrument. The films were deposited on an adhesive carbon film and analysed under vacuum. The quantification of the heavy elements was carried out with the INCA software, with a dwell time of 3 μs.

NO release measurement in solution. The release of NO in aqueous solutions performed using a tungsten lamp (60 W, 30 cm distance between the lamp and the vials) was monitored using the Griess assay. For this, 10 mg of sample was suspended in 2 mL of distilled water and put under light and orbital stirring. At each time point (0.08, 0.17, 0.25, 1, 2, 4 and 7 days), the supernatant was recovered by centrifugation at 35 700 × g (12 000 rpm, 10 min) and replaced with the same volume of fresh distilled water. The NO release from supernatants was then quantified using the Griess assay.[40] A volume of supernatant was mixed with sulfanilamide (1 mM) and *N*-(1-naphthyl)ethylenediamine (1 mM) before being measured *via* UV-vis spectroscopy. The amount of the released NO was then determined using a calibration curve previously obtained using $NaNO_2$ at concentrations ranging from 10 to 50 μM. All experimental releases were assessed over three experimental replicates and the error bars represent the mean standard error.

CN^- release measurements in solution. The release of CN^- in aqueous solutions under irradiation was quantified by photometric titration (Eurofins, Saverne, France). Samples were prepared as follows: a determined amount of composites (50–100 mg) was added to 30 mL of water in a transparent closed vial; constant irradiation was then performed using a tungsten lamp (60 W, 30 cm distance between the lamp and the vials). At each time point (1, 2, 4 and 7 days), the suspension was centrifuged, the supernatants were stored, 30 mL of water was added again, and the supernatants were then gathered (120 mL) and sent to Eurofins for the determination of the CN^- amount.

NO release modeling. The release of NO was modelled and fitted using the chemical equation associated to the NO release

and its diffusion inside the sample described in the ESI.† The equations were solved using the COMSOL software.

Results and discussion

Fig. 1 presents the step-by-step approach for the synthesis of nanocomposites $\{M_x[Fe(CN)_5(NO)]\}_y@C_6H_{11}NO_4$ (with M = Ag^+ or Fe^{2+}) *via* the growth of the corresponding cyano-bridged coordination polymers by a sequential addition of the nitroprusside and the corresponding metal ion precursors in the presence of the chitosan film. Such a strategy was previously successfully used to design chitosan-based nanocomposite beads with Prussian blue analogue nanoparticles.[33–38] As described in more details in the Experimental section, the elaboration of the cyano-bridged coordination polymer within the chitosan is performed *via* the addition of the metal ion M^{n+} (Ag^+ or Fe^{2+}) to the $-NH_2$ functionalities of chitosan and then $Na_2[Fe(CN)_5NO]\cdot 2H_2O$ (5×10^{-2} M) using methanol solutions. These successive additions were repeated 3 times with intermediate washings leading after a final air drying step to composites **1@chit** and **2@chit** as brown or light pink films, respectively, while the pristine chitosan film is white.

The IR spectra were recorded for these composites especially in the spectral window of 1800–2400 cm^{-1}, *i.e.* in the vicinity of the CN^- and NO stretching modes, which are fingerprints of the structural and electronic changes occurring in cyano-bridged coordination polymers and nitroprusside. The IR spectrum of **1@chit** shows a strong band at 2182 cm^{-1} ascribed to the $\nu(C{\equiv}N)$ stretching vibrations for the bridging (Fe^{II}–CN–Fe^{II}) mode of $Fe[Fe(CN)_5NO]$ with a shoulder at 2145 cm^{-1}, which can be ascribed to the non-bridging cyanides (Fig. 2 and 7). This band can be also seen in the IR spectrum of the bulk analogue **1**.[41] Sample **2@chit** exhibits a strong band at 2141 cm^{-1} with a shoulder at 2177 cm^{-1} ascribed to $\nu(C{\equiv}N)$ for the non-bridging and Ag^I–NC–Fe^{II} bridging modes, respectively (Fig. 2 and Fig. S1, ESI†).[27] Note that the presence of bands ascribed to the non-bridging cyanides has already been observed in the case of Prussian blue analogue nanoparticles embedded in the chitosan matrix.[33,36] The spectra of both composites show the characteristic $\nu(N{\equiv}O)$ band at 1937 and 1924 cm^{-1}, respectively, for **1@chit** and **2@chit** (Fig. 2 and 7, Fig. S1, ESI†).[39] The characteristic bands of the chitosan matrix are also present in these IR spectra beside the described bands of the coordination polymer particles, as expected.[42]

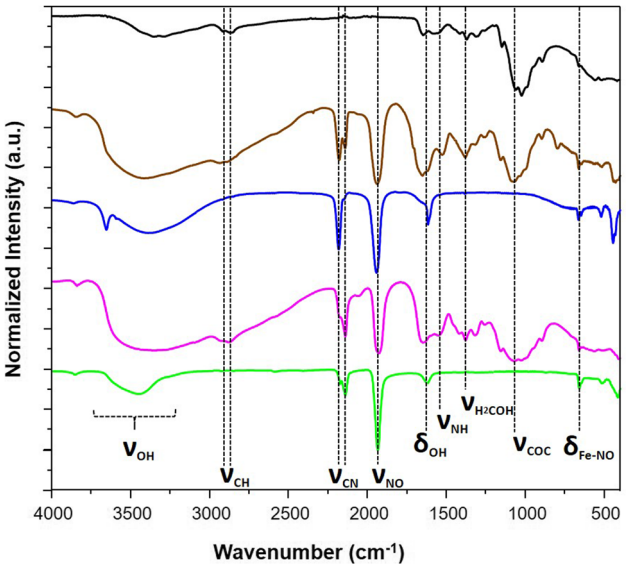

Fig. 2 IR spectra of the pristine chitosan (black), **1@chit** (brown), **1** (blue), **2@chit** (purple) and **2** (green).

The calculated coordination polymers loading from the elemental analysis are equal to 48 and 41 wt% for **1@chit** and **2@chit**, respectively. The resulting formulas obtained from an ensemble of elemental, TGA (Fig. S2 and S3, ESI†) and SEM-EDX analyses are $\{Fe[Fe(CN)_5(NO)]\}_{0.55}@C_6H_{11}NO_4$ for **1@chit** and $\{Ag_2[Fe(CN)_5(NO)]\}_{0.28}@C_6H_{11}NO_4$ for **2@chit**. The powder X-ray diffraction (PXRD) pattern for **1@chit** shows a cubic structure with an estimated cell parameter of a = 10.35 Å in accordance with the PXRD pattern of **1** (CCDC 1730892).[43] Nanocomposite **2@chit** shows a monoclinic structure with estimated cell parameters a = 7.483(6) Å, b = 6.299(2) Å, c = 12.669(6) Å, β = 114.77(3) in accordance with the PXRD pattern of **2** (CCDC 1056385) even though some discrepancies can be observed (Fig. 3).[27] Such discrepancies can be attributed to the kinetics of formation of **2** which is much faster than that of **1** and to the fact that its synthesis is carried out on chitosan that can explain an imperfect crystallization of **2** within the chitosan matrix.

To obtain information about the morphological characteristics, SEM was performed on the obtained composite and the pristine chitosan films (Fig. 4, Fig. S4, ESI†). The images demonstrate the formation of the crystalline particles of a few μm in the chitosan. The homogeneity of the composite films **1@chit** and **2@chit** can be clearly seen using EDS mapping images of iron and silver atoms (Fig. 5) both on the surface and on the transversal cuts of the films. Both of them present a homogenous distribution of Fe or Fe and Ag atoms on the

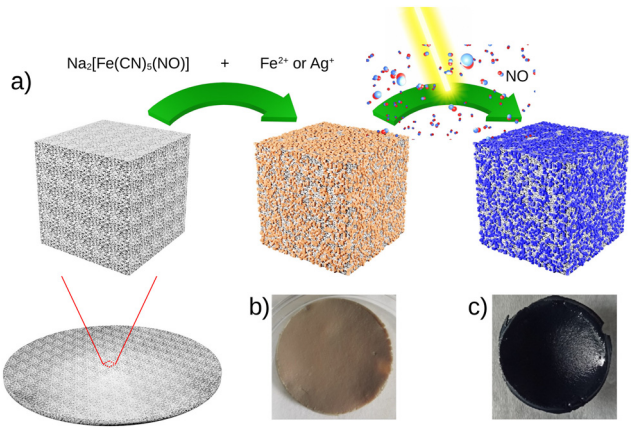

Fig. 1 (a) Synthesis of the composite materials $\{M_x[Fe(CN)_5(NO)]\}_y@C_6H_{11}NO_4$ with M = Fe^{2+} **1@chit** or Ag^+ **2@chit** followed by light irradiation and NO release, and the corresponding photographs of the composite film **1@chit** before (b) and after irradiation (c).

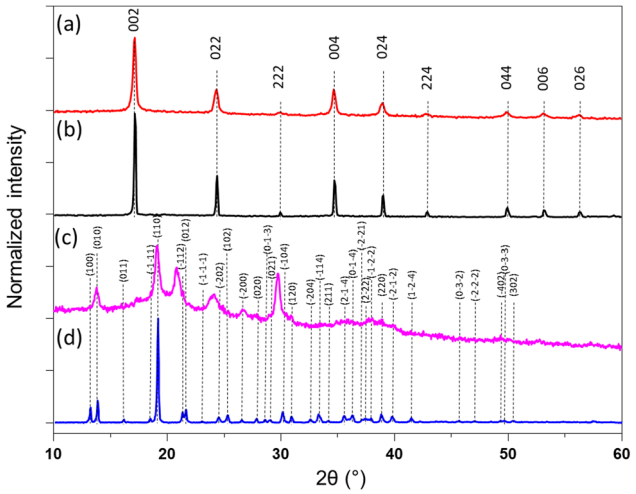

Fig. 3 (a) PXRD pattern of **1@chit**; (b) **1**; (c) **2@chit**; (d) **2**.

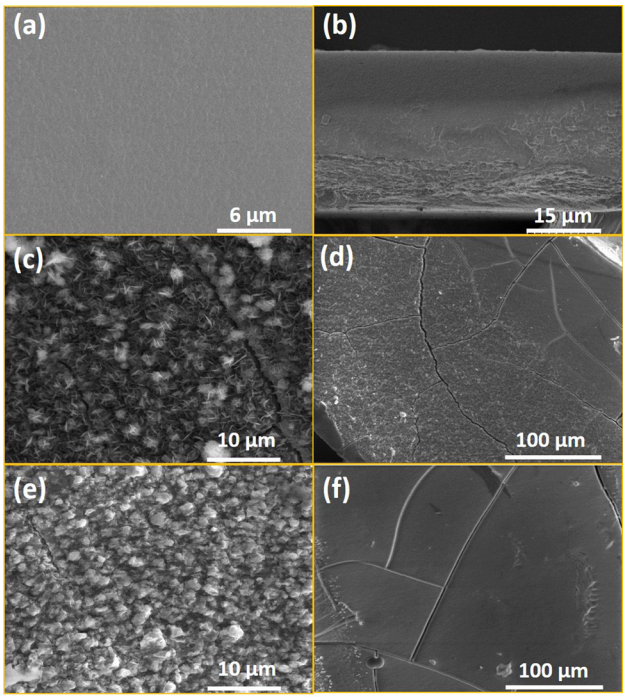

Fig. 4 SEM top film images of the chitosan film surface (a) and its transversal cut (b); (b) the **1@chit** film surface (c) and its transversal cut (d); the **2@chit** film surface (e) and its transversal cut (f).

surface (Fig. 5a and b). Transversal cuts for **2@chit** (Fig. 5d) indicate that the occurrence of silver and iron atoms is more evidenced in the first layer (*ca.* 0.15 mm) of the film's surface, indicating that the $Ag_2[Fe(CN)_5NO]$ coordination polymer particles are more dense in that location probably due to the very fast formation kinetics of this compound. On the other hand, the homogenous distribution of iron and then the $Fe[Fe(CN)_5NO]$ particles in **1@chit** can be observed in the whole width of the film (Fig. 5c).

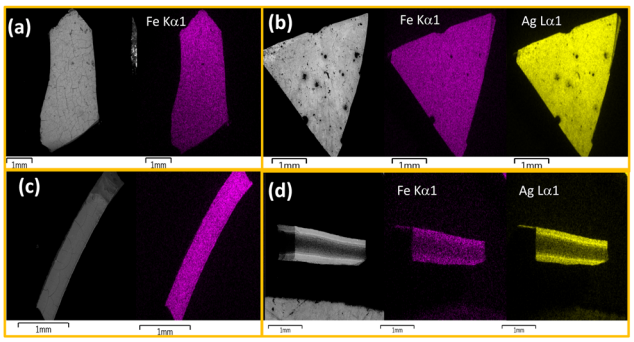

Fig. 5 SEM and SEM-EDS atomic mapping for the **1@chit** surface (a), its transversal cut (c) and the **2@chit** surface (b), its transversal cut (d). Iron atoms are shown in purple and silver one in yellow.

Previously, it has been demonstrated that the NO release for aqueous solutions of nitroprusside can be triggered either using endogenous (such as pH, glutathione or H_2O_2) or exogenous *stimuli* (such as light, X-ray or ultrasound).[14] In the present study, the NO release was triggered by light irradiation in the visible region using white light from a simple desk lamp. The measurement of NO release was performed using **1@chit** and **2@chit** dispersed in water under irradiation using a white lamp (60 W) for a period of 7 days. At each time point, the amount of the formed NO was detected by the Griess assay in water at room temperature. This analysis has previously been used for detection of NO in other NO donor systems and relies on the aerobic fast conversion of NO to NO_2^-.[44–46] The amount of cumulative NO release as a function of time (Fig. 6) indicates that the liberation of NO in water is rapid and almost linear within 1 day for both samples. After 1 day, samples continue to release NO, but much slowly. After 7 days, the saturation is not reached for **2@chit**, suggesting that the sample will still slowly produce nitric oxide beyond 7 days.

The total cumulated amounts of nitrite of 114.5 ± 5.4 and 107.9 ± 8.5 µmol g^{-1} detected after 7 days correspond to 6.5% and 10.6% of the released NO for **1@chit** and **2@chit**, respectively (Fig. 6). The maximal calculated amounts of the available

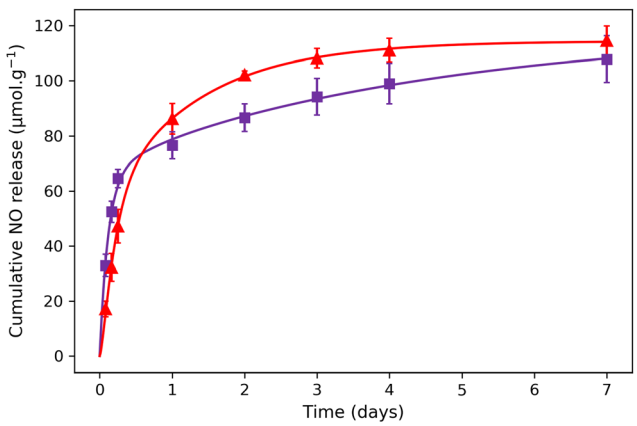

Fig. 6 NO release experimental points for (▲) **1@chit** and (■) **2@chit** under white light irradiation. The solid lines represent the theoretical fit with the model described in the ESI.†

Table 1 Amounts of released NO and CN^- detected for **1@chit** and **2@chit** 7 days after light irradiation

	1@chit	2@chit
NO release (μmol g^{-1})	114.5 ± 5.4	107.9 ± 8.5
Relative % of NO release	6.5%	10.6%
CN^- release (μmol g^{-1})	5.5 ± 1.4	202 ± 50.5
Relative % of CN^- release	6.2×10^{-2}%	4.0%

NO in these samples are 1770 μmol g^{-1} (for **1@chit**) and 1021 μmol g^{-1} (for **2@chit**) (Table 1).

We show in Table 2 different parameters for different materials reported in the literature able to deliver NO. Entries 1–3 (entry 3 relates to the present work) are related to materials using nitroprusside as the NO source, while entries 4–7 are related to materials using *N*-diazoniumdiolate and entry 8 is related to a material using the ruthenium tetraammine nitrosyl complex. The NO release is triggered by light for materials containing nitroprusside and ruthenium tetraammine nitrosyl complex, while it is triggered through pH for materials containing *N*-diazoniumdiolate. Depending on the different materials and their compositions, the quantity of NO released varies strongly from 0.14 to 920 μmol g^{-1} with maximum delivery times varying from few hours (entries 2, 4–8) to almost 1 day (entries 1, 6). The results obtained in the present study (entry 3) are in the same order of magnitude in terms of the total quantity delivered to other studies carried out for the most efficient but with much slower (by a factor of ten) kinetic release (up to 7 days), which is particularly suited to issues related to the healing of chronic wounds (Table 2).[18,19,21,44,47–49] In this perspective, it is also particularly interesting to note that for the materials containing nitroprusside, the amount of cyanide released is considerably lower in the present study (entry 3) compared with other nitroprusside-containing materials (entry 1). It should be noted that carboxymethyl chitosan/sodium alginate films loaded with *S*-nitrosoglutathione were shown to *in vitro* release NO for 168 h.[50]

The experimental NO release has been fitted using a diffusion model based on the Higuchi equation, which takes into account the formation of NO gas from the nitroprusside-containing cyano-bridged coordination polymers and then models the diffusion of NO molecules inside the chitosan matrix and their release in the solution (see the ESI† for details).[51] In the model, the NO gas formation depends on the chemical coefficient rate k_{NO} and the total number per unit of NO gas molecules, which can be released from the nitroprusside-containing cyano-bridged coordination polymers per mass unit of the latter $C_{TOT\text{-}NO}$. The diffusion time of NO gas in the chitosan matrix depends on the diffusion coefficient *D*, which is a constant rate per surface unit depending on the sample physical-chemical properties. From *D*, we can define the diffusion flux *J*, which represents the quantity of NO molecules which passes through a surface unit (see the ESI†). For sample **1@chit**, the obtained parameters gave: $D = 12553 \pm 687$ μm^2 days^{-1}, $C_{TOT\text{-}NO} = 114.6 \pm 0.8$ μmol g^{-1} and $k_{NO} = 0.331 \pm 0.014$ hour^{-1}. The experimental data for NO release for sample **2@chit** present a different behaviour compared to sample **1@chit** (see Fig. 6). As Fig. 5d shows a higher concentration of the cyano-bridged material on the surfaces for **2@chit**, we adapted the model taking into account a difference of NO concentrations between the surface ($C_{S\text{-}NO}$) and the volume ($C_{TOT\text{-}NO}$–$C_{S\text{-}NO}$). The obtained parameters gave: $D = 9670 \pm 5285$ μm^2 days^{-1}, $C_{TOT\text{-}NO} = 119.4 \pm 11.8$ μmol g^{-1}, $C_{S\text{-}NO} = 60.7 \pm 4.4$ μmol g^{-1} and $k_{NO} = 0.390 \pm 0.053$ hour^{-1}. It is important to note that the release of NO at the surface is almost instantaneous and not linked to the diffusion coefficient *D*, which induces a high error in the *D* parameter obtained from the fit. These results indicate that the diffusion coefficient *D* and the coefficient rate k_{NO} are in the same order of magnitude for both samples due to a similar matrix and the close physicochemical properties of the two nitroprusside-containing cyano-brigded coordination polymers. However, the release behaviour of NO within the composites is significantly different between both composites. The fitting of the NO release curve obtained from **1@chit** does not imply to consider a surface source term, however this term is necessary to fit the NO release curve obtained from **2@chit**. This is in agreement with the results obtained from SEM-EDS that shows a homogeneous distribution of the cyano-bridged coordination polymer in the chitosan film for **1@chit**, while a preferential location of the cyano-bridged coordination polymer in the first layer near the surface is observed for **2@chit**.

The measurement of CN^- release for samples **1@chit** and **2@chit** in aqueous solutions after irradiation for 7 days (same conditions, as for NO release experiments) was realised by photometric titration. The cumulative quantities of the released cyanides are equal to 5.5 μmol g^{-1} for **1@chit** and 202 μmol g^{-1} for **2@chit**, while the expected CN^- amounts in the hypothesis of their full release are 8850 μmol g^{-1} and 5105 μmol g^{-1}. This corresponds to 6.2×10^{-2}% and 4.0% of CN^- leaching in the solution for **1@chit** and **2@chit**, respectively (Table 1). Note that in comparison with previously published works,[44] such particularly low amount of released cyanides after NO departure in the case of composite film **1@chit** indicates the mobilisation of cyanide ligands for the rearrangement to the more stable Prussian blue networks. This fact signifies that NO may be delivered without important side cyanide release, which is promising for future biomedical applications, such as wound healing.

After being exposed to white light for 7 days, the IR spectra of composites **1@chit** and **2@chit** were recorded in order to gather the information about the fate of the coordination polymers after irradiation and a partial NO departure. A new large band at 2070 cm^{-1} clearly appeared for **1@chit** after irradiation (Fig. 7), as it can also be observed for **1** (Fig. S5, ESI†). It can be attributed to the stretching vibration of the bridging cyanides in the Fe^{II}–C≡N–Fe^{III} linkage mode attesting the formation of the Prussian blue compound.[52] Indeed, the release of NO is accompanied by a partial oxidation of Fe^{2+} to Fe^{3+} ions affording very stable Prussian blue. Note also that the relative intensity of the ν(NO) band at 1939 cm^{-1} notably decreases for **1** after irradiation. This is perfectly coherent with the results obtained by others after a white light irradiation of

Table 2 Comparison of different NO release systems found in the literature

Entry	NO-donor	Matrix	Trigger	Total NO released, μmol g^{-1}	Relative % of NO release	Relative % of CN^- release	Maximum delivery time (h)	Ref.
1	Nitroprusside	Mesoporous SiO_2 nanoparticles bearing amine functions	Blue LED	335	100	36	18	44
2	Nitroprusside	Mesoporous SiO_2 nanoparticles	—[a]	—[a]	—[a]	n.d.	3	19
3	Nitroprusside	Chitosan	White light	107–114	6.5–10.6	0.062–4	168	This work
4	*N*-Diazoniumdiolate	Mesoporous SiO_2 nanoparticles bearing amine functions	pH	2.78–920	5.8–51.7	n.a.	0.11–0.18	18
5	*N*-Diazoniumdiolate	Au nanoparticles/tiopronin	pH	0.14–40.4	2–33.4	n.a.	1.5–16	21
6	*N*-Diazoniumdiolate	SiO_2 nanoparticles/quaternary ammonium epoxides	pH	*ca.* 300	100	n.a.	24<	48
7	*N*-Diazoniumdiolate	Alkylamine-modified alginates	pH	80–550	24–100	n.a.	4[b]	47
8	Ruthenium tetra-ammine nitrosyl complex	Silica gel/isonicotinamide	White light	11.3	87	n.a.	1	49

[a] The release of nitroprusside and not NO was measured in this study precluding straight comparison. [b] NO-release half-life.

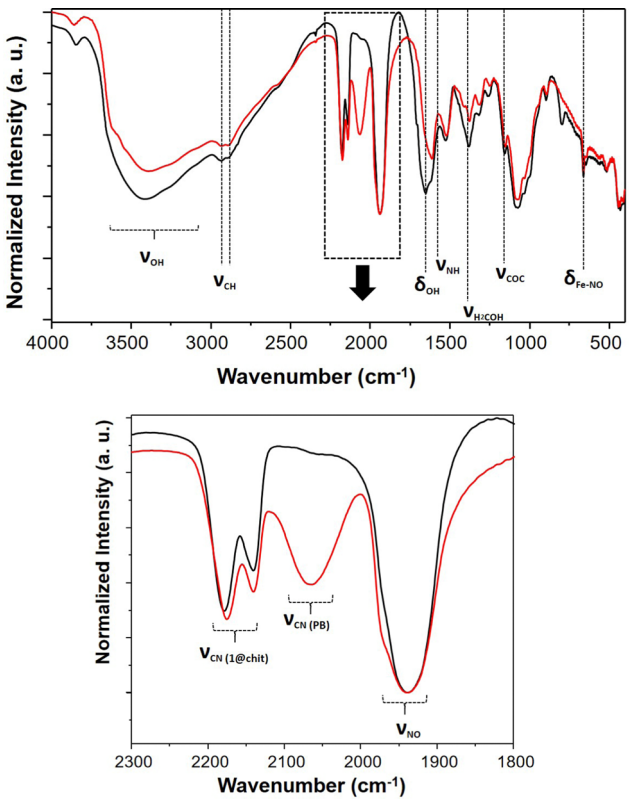

Fig. 7 IR spectra of **1@chit** before (black) and after (red) NO release; (up) spectral window 4000–400 cm^{-1}, (down) spectral window 2300–1800 cm^{-1}.

the respective bulk coordination polymer **1**.[28] Moreover, the absorption spectrum in the visible region of **1@chit** after irradiation demonstrates the appearance of a broad band typical for Prussian blue at *ca.* 730 nm occurring due to the Fe^{3+} to Fe^{2+} electron transfer (Fig. S6, ESI†).[53]

For the composite film **2@chit**, a new band appears at *ca.* 2055 cm^{-1} in the IR spectrum, which corresponds to the stretching vibration of the cyanide groups in the bridging mode Fe^{II}–C≡N–Ag^{I} due to the formation of the Prussian blue analogue $Ag_4[Fe(CN)_6]$ (Fig. S1, ESI†).[54] Note that in this case, no Fe^{2+} to Fe^{3+} oxidation occurs since ν(CN) for the Fe^{III}–C≡N–Ag^{I} mode is expected at 2092 cm^{-1}.[55] Interestingly, the related bulk compound **2** does not release NO upon irradiation and no new bands have been observed in its IR spectrum taken after irradiation under similar conditions. Thus, for both nanocomposites, the NO departure is accompanied with a self-restructuration of the material leading to the formation of the corresponding cyano-bridged coordination polymers limiting the concomitant release of cyanide. However, this reaction seems more efficient for **1@chit** than **2@chit**, as the amount of cyanide release is strongly limited for the former.

Conclusions

To summarize, in this work, we showed that cyano-bridged coordination polymer particles $Fe^{II}[Fe^{II}(CN)_5(NO)]$ or $Ag_2^{I}[Fe^{II}(CN)_5(NO)]$ can be grown by the step-by-step coordination of Fe^{2+} or Ag^+ and $[Fe(CN)_5(NO)]^{2-}$ precursors inside the chitosan film as a matrix. Their morphological and structural characterisation demonstrated that those composite materials are made of *ca.* 50–50 wt% of the cyano-bridged coordination polymer and chitosan, the formers being present as microcrystalline components. Note that while $Fe^{II}[Fe^{II}(CN)_5(NO)]$ is shown to be homogeneously distributed in the chitosan film, the Ag_2^{I} $[Fe^{II}(CN)_5(NO)]$-containing film exhibits a preferential location of the particles in the first layer near the surface of the chitosan film. Continuous irradiation of both nanocomposites using a desk lamp in aqueous media initiates the slow NO release, which was measured during the experimentation time. It indicates a maximum amount of 6.5 and 10.6% released 7 days after irradiation for **1@chit** and **2@chit**, respectively. Modelling of the NO release for **1@chit** can be obtained satisfactorily without considering a specific contribution of the surface, while for **2@chit**, the surface contribution has to be taken into account. This is in agreement with a higher amount of the cyano-bridged coordination material on the

surfaces of the chitosan film for **2@chit**. The infrared and absorption spectroscopies performed before and after irradiation demonstrated that a structural rearrangement of the cyano-bridged coordination polymers leading to the formation of Prussian blue or the Prussian blue analogue $Ag_2[Fe(CN)_6]$ particles has occurred after NO departure. Such a self-structuring of the composite associated with chitosan allows the concomitant release of cyanides to be limited, which is shown to be particularly efficient in the case of **1@chit**. Such a strategy allowing the successful release of NO from nitroprusside-based composites while limiting the release of cyanide opens interesting opportunities for different potential applications where delivery of small quantities of NO for a long period of time is needed without side effects linked to cyanide.

Author contributions

Conceptualization: N. T., F. Q., J. La., and Y. G.; data curation: M. G., N. W. M. A. P., and G. F.; formal analysis: G. F.; funding acquisition: Y. G.; investigation: M. G., N. W. M. A. P., S. S., and G. F.; methodology: G. F.; project administration: J. La. and Y. G.; resources: S. S.; software: G. F. supervision: N. T., F. Q., J. La., and Y. G.; validation: M. G., N. W. M. A. P., and S. S.; writing – original draft: S. S., G. F., and Y. G.; writing – review & editing: N. T., J. La., J. Lo, and Y. G.

Conflicts of interest

There are no conflicts to declare.

Acknowledgements

The authors thank the Institut Carnot Chimie Balard Cirimat and SATT AxLR for financial support.

Notes and references

1 S. P. Nichols, *et al.*, *Adv. Drug Delivery Rev.*, 2012, **64**, 1177–1188.
2 C. Szabo, *Nat. Rev. Drug Discovery*, 2016, **15**, 185–203.
3 S. Korde Choudhari, *et al.*, *World J. Surg. Oncol.*, 2013, **11**, 118.
4 A. P. Veith, *et al.*, *Adv. Drug Delivery Rev.*, 2019, **146**, 97–125.
5 D. A. Popowich, *et al.*, *Vascular*, 2007, **15**, 324–335.
6 D. O. Schairer, *et al.*, *Virulence*, 2012, **3**, 271–279.
7 R. Y. Pelgrift, *et al.*, *Adv. Drug Delivery Rev.*, 2013, **65**, 1803–1815.
8 X. Zhu, *et al.*, *Nano Today*, 2014, **9**, 478–498.
9 A. Simchi, *et al.*, *Nanomedicine*, 2011, **7**, 22–39.
10 Y. Yang, *et al.*, *Biosurf. Biotribol.*, 2015, **1**, 177–201.
11 R. Ahmed, *et al.*, *Biomed. Pharmacother.*, 2022, **149**, 112707.
12 J. L. Harding, *et al.*, *J. Mater. Chem. B*, 2014, **2**, 2530–2536.
13 L. Tan, *et al.*, *Colloids Surf., B*, 2021, **199**, 111508.
14 W. Fan, *et al.*, *Angew. Chem., Int. Ed.*, 2018, **57**, 8383–8394.
15 G. Jin, *et al.*, *Adv. Healthcare Mater.*, 2021, **10**, 2001550.
16 J. Cheng, *et al.*, *Front. Chem.*, 2019, **7**, 530.
17 D. A. Riccio, *et al.*, *Chem. Soc. Rev.*, 2012, **41**, 3731–3741.
18 J. H. Shin, *et al.*, *J. Am. Chem. Soc.*, 2007, **129**, 4612–4619.
19 A. Farooq, *et al.*, *J. Colloid Interface Sci.*, 2016, **478**, 127–135.
20 A. C. McKinlay, *et al.*, *J. Am. Chem. Soc.*, 2008, **130**, 10440–10444.
21 M. A. Polizzi, *et al.*, *Langmuir*, 2007, **23**, 4938–4943.
22 R. V. Pinto, *et al.*, *Angew. Chem., Int. Ed.*, 2020, **59**, 5135–5143.
23 A. C. McKinlay, *et al.*, *Chem. Mater.*, 2013, **25**, 1592–1599.
24 A. R. Butler, *et al.*, *Chem. Soc. Rev.*, 1987, **16**, 361–380.
25 P. Coppens, *et al.*, *Chem. Rev.*, 2002, **102**, 861–884.
26 A. Gómez, *et al.*, *Powder Diffr.*, 2007, **22**, 27–34.
27 J. Rodríguez-Hernández, *et al.*, *Inorg. Chim. Acta*, 2015, **428**, 51–56.
28 P. M. Crespo, *et al.*, *J. Photochem. Photobiol., A*, 2021, **412**, 113244.
29 G. A. F. Roberts, in *Chitin Chemistry*, ed. M. E., UK, London, 1992, pp. 54–84.
30 M. N. V. R. Kumar, *et al.*, *Chem. Rev.*, 2004, **104**, 6017–6084.
31 R. Valentin, *et al.*, *New J. Chem.*, 2003, **27**, 1690–1692.
32 F. Quignard, *et al.*, *New J. Chem.*, 2008, **32**, 1300–1310.
33 Y. Guari, *et al.*, *Chem. Commun.*, 2006, 2613–2615, DOI: **10.1039/B602460B**,.
34 J. Larionova, *et al.*, *Angew. Chem., Int. Ed.*, 2008, **47**, 8236–8240.
35 Y. Guari, *et al.*, *Dalton Trans.*, 2008, 3658–3660, DOI: **10.1039/B808221A**,.
36 B. Folch, *et al.*, *Phys. Chem. Chem. Phys.*, 2010, **12**, 12760–12770.
37 E. Chelebaeva, *et al.*, *Nanoscale*, 2011, **3**, 1200–1210.
38 A. Tokarev, *et al.*, *New J. Chem.*, 2013, **37**, 3420–3432.
39 D. F. Mullica, *et al.*, *J. Crystallogr. Spectrosc. Res.*, 1991, **21**, 81–85.
40 D. Giustarini, *et al.*, *Methods in Enzymology*, Academic Press, 2008, vol. 440, pp. 361–380.
41 J. Balmaseda, *et al.*, *J. Phys. Chem. B*, 2003, **107**, 11360–11369.
42 I. F. M. Rumengan, *et al.*, *IOP Conf. Ser.: Earth Environ. Sci.*, 2017, **89**, 012028.
43 E. Reguera, *et al.*, *Hyperfine Interact.*, 1993, **77**, 1–10.
44 P. M. Silva Filho, *et al.*, *Mol. Pharmaceutics*, 2019, **16**, 2912–2921.
45 X. Zhou, *et al.*, *Acta Biomater.*, 2017, **54**, 128–137.
46 T. Feng, *et al.*, *Biomaterials*, 2019, **214**, 119213.
47 M. J. R. Ahonen, *et al.*, *Biomacromolecules*, 2018, **19**, 1189–1197.
48 A. W. Carpenter, *et al.*, *Biomacromolecules*, 2012, **13**, 3334–3342.
49 F. G. Doro, *et al.*, *J. Colloid Interface Sci.*, 2007, **307**, 405–417.
50 K. Razmjooee, *et al.*, *Biomed. Mater.*, 2022, **17**, 055013.
51 J. Siepmann, *et al.*, *Int. J. Pharm.*, 2011, **418**, 6–12.
52 S. N. Ghosh, *J. Inorg. Nucl. Chem.*, 1974, **36**, 2465–2466.
53 R. Koncki, *et al.*, *Anal. Chem.*, 1998, **70**, 2544–2550.
54 S. Sharma, *et al.*, *Mater. Sci. Eng., C*, 2020, **113**, 110982.
55 S. Mukherjee, *et al.*, *ACS Biomater. Sci. Eng.*, 2020, **6**, 690–704.

